

# Observation of superconductivity and surface noise using a single trapped ion as a field probe

K. Lakhmanskiy<sup>1,\*</sup>, P. C. Holz<sup>1,\*</sup>, D. Schärfl<sup>1</sup>, B. Ames<sup>1</sup>, R. Assouly<sup>1</sup>,  
T. Monz<sup>1</sup>, Y. Colombe<sup>1</sup>, R. Blatt<sup>1,2</sup>

<sup>1</sup>*Institut für Experimentalphysik, Universität Innsbruck, Technikerstrasse 25, 6020 Innsbruck, Austria*

<sup>2</sup>*Institut für Quantenoptik und Quanteninformation,*

*Österreichische Akademie der Wissenschaften, Technikerstr. 21 A, 6020 Innsbruck, Austria*

*\*these authors contributed equally to this work*

(Dated: December 14, 2024)

Measuring and understanding electric field noise from bulk material and surfaces is important for many areas of physics. In this work, we introduce a method to detect in situ different sources of electric field noise using a single trapped ion as a sensor. We demonstrate the probing of electric field noise as small as  $S_E = 5.2(11) \times 10^{-16} \text{V}^2 \text{m}^{-2} \text{Hz}^{-1}$ , the lowest noise level observed with a trapped ion to our knowledge. Our setup incorporates a controllable noise source utilizing a high-temperature superconductor. This element allows us, first, to benchmark and validate the sensitivity of our probe. Second, to probe non-invasively bulk properties of the superconductor, observing for the first time a superconducting transition with an ion. For temperatures below the transition, we use our setup to assess different surface noise processes. The measured noise shows a crossover regime in the frequency domain, which cannot be explained by existing surface noise models. Our results open perspectives for new models in surface science and pave the way to test them experimentally.

Electric field noise provides insights into microscopic processes, and imposes limitations to experimental systems. In particular, electric field noise in close proximity to surfaces creates obstacles for near-field measurements [1, 2], experiments with nitrogen-vacancy centers [3], Casimir effect studies [4], gravitational-wave detectors [5], and ion trapping experiments [6]. It has been suggested to employ the high sensitivity of trapped ions to electric field noise as a new tool in surface science [7]. Trapped ions have been used to study the dependence of electric field noise on frequency, trap temperature and ion-surface distance [8–14] and have been combined with the analysis and removal of surface contaminants [14–16]. In this work, we use a surface-electrode ion trap containing a high-temperature superconductor to investigate not only surface noise but also bulk material properties. We operate the trap in two distinct regimes, above and below the critical temperature  $T_c$  of its superconducting electrodes. Above  $T_c$ , the electric field noise sensed by the ion originates from the bulk resistance of two long electrodes; below  $T_c$ , this resistance vanishes and the ion probes the noise from the surface of the trap. In this way, we compare different sources of electric field noise in situ, with a single device. The capability to probe the resistivity of the superconductor with an ion also allows us to observe the superconducting transition non-invasively, without direct electrical probing. This constitutes the first observation of superconductivity using an ion as a probe. Conventional superconductors have been used in the past as ion trap material to study electric field noise above and below  $T_c$  [17, 18]. In these studies, however, the onset of superconductivity did not lead to a measurable modification of the electric field noise at the ion.

Important sources of electric field noise in trapped

ion experiments are technical noise, Johnson-Nyquist (Johnson) noise, and surface noise. Technical noise is related to control devices like power supplies as well as to electromagnetic interference from nearby electronics. Johnson noise is caused by thermal motion of charge carriers in conductors [19]. Surface noise is thought to arise from different physical processes related to the surface material [6]. We measure the frequency spectrum and temperature dependence of the electric field noise to differentiate between these noise sources.

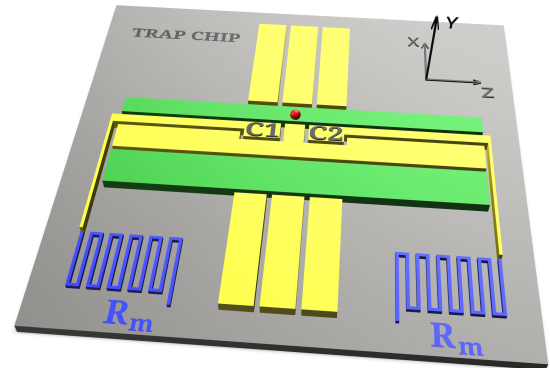


FIG. 1. Schematic illustration of the trap electrodes. DC (yellow) and RF (green) electrodes confine a single ion (red sphere) in the trap center above the surface. Two central DC electrodes C1, C2 are connected to meander resistors  $R_m$  (blue) made of YBCO, integrated to the trap chip.

Our single ion probe is confined in a linear surface-electrode Paul trap (Fig. 1). A sapphire substrate supports 50 nm-thick electrodes made of  $\text{YBa}_2\text{Cu}_3\text{O}_7$  (YBCO), a high-temperature superconductor with a crit-

ical temperature  $T_c \approx 85$  K. To ensure operability of the trap above  $T_c$  the electrodes are covered with 200 nm of gold. The key feature of the trap is a pair of electrodes C1 and C2 near the trap center, connected to two identical meander-shaped structures. These meanders are made of YBCO only, without gold coating. Below  $T_c$  the resistance  $R_m$  of each meander is negligible. Above  $T_c$  the meanders' resistance  $R_m$  gives rise to Johnson noise, which translates to electric field noise at the trap center that can be sensed with an ion. This noise source can be switched on and off by adjusting the trap chip temperature. The geometry of electrodes C1 and C2 is designed such that electric fields from correlated voltages cancel out at the center of the trap,  $\mathbf{E}^{(C1)}(\mathbf{r}=0) = -\mathbf{E}^{(C2)}(\mathbf{r}=0)$ , which minimizes the influence of pickup from the RF electrode by C1 and C2. However, the uncorrelated Johnson noise in the meanders adds up, leading to an electric field noise  $S_E = S_E^{(C1)} + S_E^{(C2)}$ .

The trap chip is mounted on a heatable copper stage that is thermally isolated from the environment. The trap chip temperature, measured with a Si diode sensor, can be set in the range  $T = (10 - 200)$  K, while the low-pass filter boards and RF resonator stay at a nearly constant temperature  $T_f \approx (10 - 14)$  K. This thermal decoupling ensures that noise from off-chip sources, e. g., Johnson noise from the low-pass filters or external technical noise attenuated by the filters, is nearly independent of the trap chip temperature. We determine the critical temperature  $T_c$  by means of a 4-wire measurement of  $R_m$  using a third on-chip YBCO meander (not shown in Fig. 1) identical to the ones connected to C1 and C2. This DC measurement of  $R_m$  is used to calculate the Johnson noise in the MHz regime for  $T > T_c$  where the skin depth  $\zeta$  is orders of magnitude larger than the YBCO film thickness (Supplemental Material [20]).

The experiment is performed in a cryogenic apparatus [21, 22]. We confine a single  $^{40}\text{Ca}^+$  ion at a distance  $d = 225 \mu\text{m}$  above the surface of the trap chip using static (DC) and radio-frequency (RF) electric fields. An RF drive voltage  $V_{\text{RF}} \sim 230$  V at  $\omega_{\text{RF}} = 2\pi \times 17.6$  MHz provides radial confinement  $\omega_{x,y} \sim 2\pi \times 3$  MHz in the  $xy$  plane. The axial motional frequency  $\omega_z$  is varied in the range  $\omega_z = 2\pi \times (0.4 - 1.8)$  MHz by changing the DC voltages. Electric field noise couples to the ion and adds phonons to its motional state at a rate  $\Gamma_h$ . The relation between this heating rate  $\Gamma_h$  and the electric field noise spectral density  $S_E(\omega)$  at the position of the ion is [6]

$$\Gamma_h = \frac{q^2}{4m\hbar\omega} S_E(\omega), \quad (1)$$

with  $\hbar$  the reduced Planck constant,  $q$  and  $m$  the ion's charge and mass, and  $\omega$  its motional frequency. The ion is prepared in the ground state of its axial mode by Doppler and subsequent sideband laser cooling. A narrow linewidth 729 nm laser tuned to the  $S_{1/2} \leftrightarrow D_{5/2}$  quadrupole transition is used to measure  $\Gamma_h$  with the

sideband ratio method [23]. The measurement uncertainties of  $\Gamma_h$  in our experiments are limited by quantum projection noise [24].

In a first study, we detect non-invasively the superconducting transition of YBCO using a single trapped ion as a probe. For this, the ion's heating rate  $\Gamma_h$  is measured for different trap chip temperatures while keeping the axial frequency constant  $\omega_z \approx 2\pi \times 1.0$  MHz, see Fig. 2. Below  $T_c$ , the heating rate increases slowly from

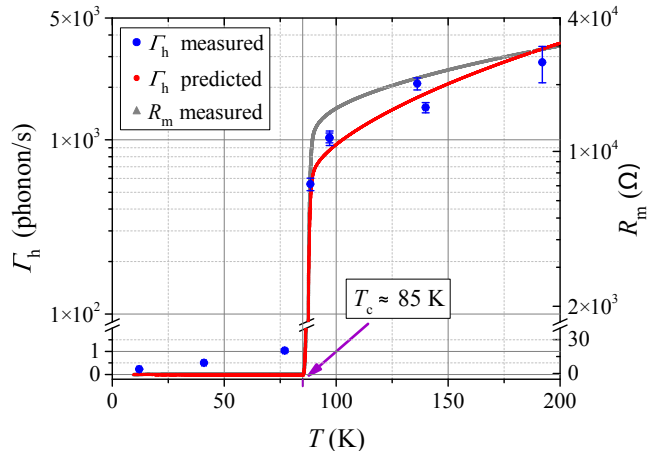


FIG. 2. Observation of the superconducting transition of YBCO with a trapped ion. Blue dots show the measured ion motional heating rate  $\Gamma_h$  as a function of trap chip temperature  $T$  for a trap frequency  $\omega_z \approx 2\pi \times 1.0$  MHz. The measured meander resistance  $R_m$  (gray data) is used to calculate the motional heating rate expected from Johnson noise in the meanders connected to C1 and C2 (red data). Note the break in the vertical axes.

$\Gamma_h = 0.23(2)$  phonons/s to  $\Gamma_h = 1.03(8)$  phonons/s between  $T = 12$  K and  $T = 77$  K. From  $T = 77$  K to  $T = 89$  K the heating rate increases by roughly a factor 500 to  $\Gamma_h = 556(46)$  phonons/s. This sudden increase coincides with the superconducting transition at  $T_c \approx 85$  K, as evidenced by the 4-wire resistance measurement (Fig. 2, gray data). For  $T > T_c$ , we show that the ion heating rate corresponds to what is expected from Johnson noise in the YBCO meanders connected to C1 and C2. The electric field spectral density of Johnson noise is given by [6, 25, 26]

$$S_E^{(\text{JN})} = \frac{4k_B T R(\omega, T)}{\delta_c^2}, \quad (2)$$

where  $k_B$  is Boltzmann's constant,  $T$  the temperature of the resistor causing the noise,  $R$  its resistance, and  $\delta_c$  a geometry-dependent characteristic distance [6]. We calculate  $\delta_c = 5.1$  mm for electrodes C1 and C2 from trap simulations [27]. Since the meanders are located directly on the trap chip, filter effects can be neglected, i.e.,  $R(\omega, T) = R_m(T)$ . Based on the resistance and temperature measurements we calculate

the expected heating rate from Eqs. (1, 2) (Fig. 2, red data). The measured heating rates are consistent with the expected values, with an average deviation  $\bar{\Delta} = 1.9$ .  $\bar{\Delta} = \langle |I_h^{(\text{meas})} - I_h^{(\text{exp})}| / \sigma \rangle$ , where  $I_h^{(\text{meas})}$  and  $I_h^{(\text{exp})}$  are the measured and expected heating rates, and  $\sigma$  is the standard deviation of an individual data point.

In a second study, we measure the spectrum of the electric field noise for trap chip temperatures above and below  $T_c$ . Above the transition we confirm the white noise nature of the engineered Johnson noise. For this, the heating rate is measured as a function of the trap frequency  $\omega_z$  for two different temperatures  $T = 97$  K and  $T = 140$  K, see Fig. 3. The solid lines show the pre-

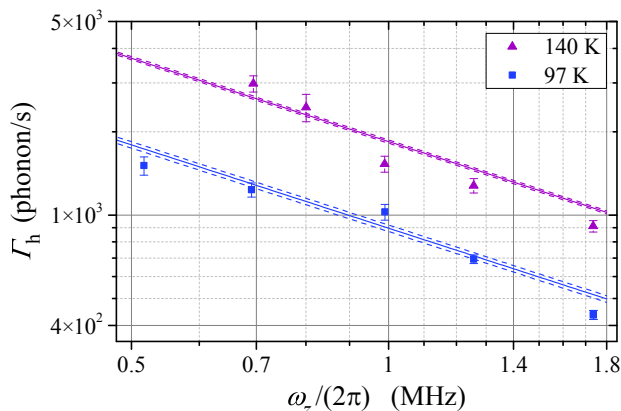


FIG. 3. Heating rate  $\Gamma_h$  as function of trap frequency for trap chip temperatures  $T = (97, 140)$  K  $> T_c$ . Solid lines are predictions for Johnson noise from the meander resistance  $R_m$ . Dashed lines reflect the 1 K uncertainty in the temperature measurement.

dicted heating rate calculated from the measured resistance  $R_m$  using equations (1),(2). The measured data show good agreement with the calculated curves with an average deviation  $\bar{\Delta} = 2.06$  for  $T = 97$  K and  $\bar{\Delta} = 2.12$  for  $T = 140$  K. For  $T < T_c$ , the heating rate spectrum is measured at three different temperatures  $T = (12, 41, 77)$  K (Fig. 4) [28]. The lowest measured heating rate is  $\Gamma_h = 0.051(10)$  phonons/s at  $T = 12$  K and  $\omega_z = 2\pi \times 1.51$  MHz which corresponds to an electric field spectral density  $S_E = 5.2(11) \times 10^{-16}$  V<sup>2</sup>m<sup>-2</sup>Hz<sup>-1</sup>, see Eq. (1). To our knowledge this is the lowest electric field noise measured with a trapped ion to date [6].

To confirm that the main origin of the measured ion heating rate for  $T < T_c$  is surface noise, we exclude other possible noise sources. Specifically, we rule out external technical noise which is independent of the trap chip temperature, in contrast to the measured heating rates; Johnson noise from filters, wiring and trap electrodes is calculated to be at least two orders of magnitude smaller than the smallest noise we measure; finally, repeating the experiment without superconducting YBCO meanders

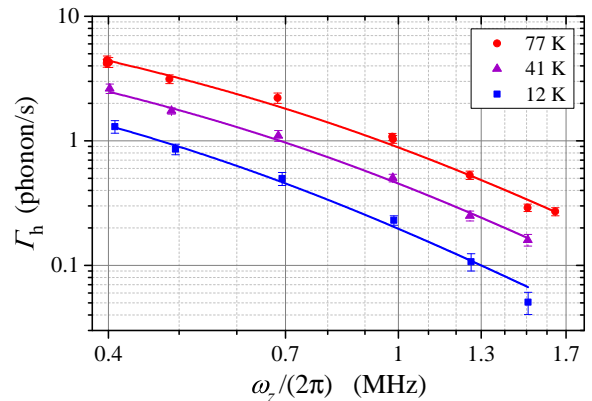


FIG. 4. Heating rate as function of trap frequency for trap chip temperatures  $T = (12, 41, 77)$  K  $< T_c$ . The solid lines are a fit to the data with the TLF model, Eq. (4).

shows that these do not contribute to the heating rate for  $T < T_c$  within the uncertainty of our measurement. The above arguments, detailed in the Supplemental Material [20], imply that the noise causing the ion's motional heating below  $T_c$  originates at the surface of the trap.

In the remainder of this Letter we analyze the spectral properties and temperature dependence of the surface noise observed below  $T_c$  (Fig. 4). We compare the data with the class of two-level fluctuator models (TLF) and an adatom diffusion model (AD) [6]. TLF models consider real or effective particles undergoing random transitions between two quantum states with different electric dipole moment. The AD model describes electric field noise arising from the diffusion of adatoms with a static dipole moment on the chip surface. Within a finite frequency range, both the class of TLF models and the AD model motivate a power law fit

$$\Gamma_h = c \omega_z^{-\alpha}. \quad (3)$$

We find a power-law exponent  $\alpha \approx 2$  for all three data sets (Tab. I), corresponding to a  $1/f$  frequency scaling of the electric field noise  $S_E$ . The exponent is close to the ones reported in Refs. [12, 13], where a  $1/d^4$  distance scaling of the heating rate was found, indicative of surface noise. However, a closer examination of the frequency dependence in the data of Fig. 4 reveals a change in the local power law exponent  $\alpha$  around 0.8 MHz, which indicates a crossover between low- and high-frequency domains. This behavior is predicted by TLF models. Transitions between the TLF states at a rate  $\omega_0$  induced either by thermal activation or quantum tunneling lead to electric field fluctuations with a spectral density [6]

$$S_E^{(\text{TLF})}(\omega) = A \frac{\omega_0}{\omega_0^2 + \omega^2}. \quad (4)$$

The solid lines in Fig. 4 show a TLF fit to the heating rate

$T$	$\alpha$	$c$	$\chi^2_{\text{power law}}$	$\chi^2_{\text{TLF model}}$
12 K	2.3(2)	0.18(2)	2.9	1.3
41 K	2.0(1)	0.42(3)	2.4	0.8
77 K	1.9(1)	0.77(6)	6.0	2.3

TABLE I. Results of a power law fit, Eq. (3), to the three data sets shown in Fig. 4. The reduced chi squared for the power law fit and the fit with the TLF model, Eq. (4), is shown in the fourth and fifth column, respectively.

data below  $T_c$ . The TLF models are in better agreement with our data than the power law, Eq. (3), using a fit with two adjustable parameters for both models (Tab. I). The TLF fit parameters are shown in Fig. 5 for the three temperatures  $T = (12, 41, 77)$  K. We find the crossover

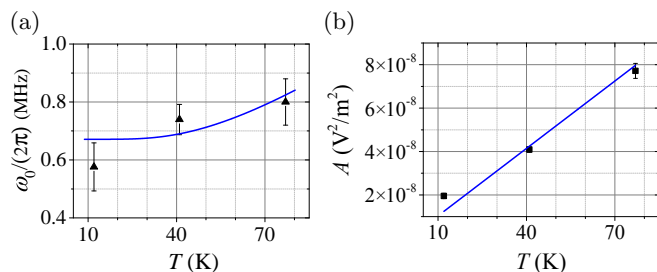


FIG. 5. Results from the fit with the TLF model, Eq. (4), to the heating rate data in Fig. 4. (a) Crossover frequency  $\omega_0(T)$  as a function of trap chip temperature  $T$ . The solid line is a fit with the expected temperature dependence, Eq. (5). (b) Magnitude prefactor  $A(T)$  as a function of  $T$ . The solid line is a linear fit (offset fixed to zero).

frequency in the range  $\omega_0 = 2\pi \times (0.6 - 0.8)$  MHz, with a slight dependence on the temperature, see Fig. 5 (a). The data is consistent with a TLF model dominated by quantum tunneling, where the crossover occurs at [29]

$$\omega_0(T) = \omega_0(T=0) \coth\left(\frac{T_0}{2T}\right), \quad (5)$$

where  $k_B T_0$  is the activation energy of the fluctuator. From a fit of the crossover frequency data in Fig. 5 (a) with Eq. (5) we derive a characteristic temperature  $T_0 = 165(65)$  K.  $T_0$  is higher than all temperatures at which we probe the system, in agreement with the assumption that quantum tunneling causes the TLF state fluctuations.

The dominant temperature dependence of the spectrum given by Eq. (4), scales as  $A(T) \propto \cosh^{-2}(T_0/2T)$  [6]. This dependence cannot be matched with the magnitude data in Fig. 5 (b). Averaging over a distribution of fluctuators can lead to a linear dependence on temperature with [6]

$$\overline{S}_E^{(\text{TLF})}(\omega) \propto T/\omega^2. \quad (6)$$

Our data in Fig. 5 (b) do not agree well with a linear fit with fixed zero offset, as evidenced by the reduced

chi squared  $\chi^2 = 18.9$ . Also, the averaged TLF model Eq. (6) does not support a crossover in the frequency dependence. Consequently, standard TLF models [6] correctly describe the frequency dependence, Fig. 5 (a), but fail to describe the temperature dependence, Fig. 5 (b).

The second surface noise model predicting a crossover region with local power law exponent  $\alpha \approx 2$  is the adatom diffusion model. In this model, the crossover frequency occurs at  $\omega_0 = D/d^2$  [6]. For typical values of the diffusion constant  $D \sim 10^{-7} \text{m}^2/\text{s}$  [30] and our surface-ion separation  $d = 225 \mu\text{m}$ , we calculate a crossover frequency  $\omega_0 \sim 2\pi \times 0.3$  Hz that is 6 orders of magnitude smaller than the value  $\omega_0 \approx 2\pi \times 0.8$  MHz we observe. Diffusion of adatoms can therefore be excluded as origin of the noise that we measure.

In conclusion, we have used a single trapped ion as a probe for bulk and surface properties of materials, achieving the highest sensitivity to electric field noise with a single ion reported to date. We employed our ion field probe to measure non-invasively the superconducting transition of YBCO. This technique could be used in the future for the characterization of samples that cannot be subjected to a direct resistance measurement, like delicate structures or topologies that cannot be connected, e.g., loops. Below the transition we measured surface noise with a crossover of the power-law exponent in the frequency domain. Such a behavior is generally expected [31] and predicted, e.g., by TLF models, but has not been observed experimentally before. The temperature dependence of our data, however, cannot be understood with existing TLF models. Our results, together with other recent studies of noise scaling with ion-electrode distance [12, 13] and chemical composition of surface materials [14–16], gives new input for understanding the origin of surface noise. The observation of a superconducting transition with an ion can be considered as a first step towards developing trapped-ion field probes capable of detecting and characterizing electrical bulk properties of solids. In addition, our work paves the way for the use of high-temperature superconductors for large scale ion-based quantum processors [32], where low-resistance trap electrodes will become important.

## ACKNOWLEDGMENTS

We thank Muir Kumph and Peter Rabl for discussions, Philipp Schindler and the quantum information experiment team for technical assistance. We acknowledge financial support by the Austrian Science Fund (FWF) through projects P26401-N20 (Q-SAIL) and F4016-N23 (SFB FoQuS), by the Institut für Quanteninformatik GmbH, and by the Office of the Director of National Intelligence (ODNI), Intelligence Advanced Research Projects Activity (IARPA), through the Army Re-

search Office grant W911NF-10-1-0284. All statements of fact, opinion or conclusions contained herein are those of the authors and should not be construed as representing the official views or policies of IARPA, the ODNI, or the U.S. Government.

- 
- [1] B. C. Stipe, H. J. Mamin, T. D. Stowe, T. W. Kenny, and D. Rugar, *Phys. Rev. Lett.* **87**, 096801 (2001).
- [2] S. Lekkala, N. Hoepker, J. A. Marohn, and R. F. Loring, *J. Chem. Phys.* **137**, 124701 (2012).
- [3] M. Kim, H. J. Mamin, M. H. Sherwood, K. Ohno, D. D. Awschalom, and D. Rugar, *Phys. Rev. Lett.* **115**, 087602 (2015).
- [4] W. J. Kim, A. O. Sushkov, D. A. R. Dalvit, and S. K. Lamoreaux, *Phys. Rev. A* **81**, 022505 (2010).
- [5] S. E. Pollack, S. Schlamminger, and J. H. Gundlach, *Phys. Rev. Lett.* **101**, 071101 (2008).
- [6] M. Brownnutt, M. Kumph, P. Rabl, and R. Blatt, *Rev. Mod. Phys.* **87**, 1419 (2015).
- [7] D. Hite, Y. Colombe, A. Wilson, D. Allcock, D. Leibfried, D. Wineland, and D. Pappas, *MRS Bull.* **38**, 826 (2013).
- [8] Q. A. Turchette, K. M. M. King, D. Leibfried, D. M. Meekhof, C. J. Myatt, M. A. Rowe, C. A. Sackett, C. S. Wood, W. M. Itano, C. Monroe, and D. J. Wineland, *Phys. Rev. A* **61**, 063418 (2000).
- [9] L. Deslauriers, S. Olmschenk, D. Stick, W. K. Hensinger, J. Sterk, and C. Monroe, *Phys. Rev. Lett.* **97**, 103007 (2006).
- [10] J. Labaziewicz, Y. Ge, D. R. Leibbrandt, S. X. Wang, R. Shewmon, and I. L. Chuang, *Phys. Rev. Lett.* **101**, 180602 (2008).
- [11] C. D. Bruzewicz, J. M. Sage, and J. Chiaverini, *Phys. Rev. A* **91**, 041402 (2015).
- [12] J. A. Sedlacek, A. A. Greene, J. Stuart, R. McConnell, C. D. Bruzewicz, J. M. Sage, and J. Chiaverini, *Phys. Rev. A* **97**, 020302 (2018).
- [13] I. A. Boldin, A. Kraft, and C. Wunderlich, *Phys. Rev. Lett.* **120**, 023201 (2018).
- [14] D. A. Hite, K. S. McKay, S. Kotler, D. Leibfried, D. J. Wineland, and D. P. Pappas, *MRS Advances* **2**, 2189 (2017).
- [15] D. A. Hite, Y. Colombe, A. C. Wilson, K. R. Brown, U. Warring, R. Jördens, J. D. Jost, K. S. McKay, D. P. Pappas, D. Leibfried, and D. J. Wineland, *Phys. Rev. Lett.* **109**, 103001 (2012).
- [16] N. Daniilidis, S. Gerber, G. Bolloten, M. Ramm, A. Ransford, E. Ulin-Avila, I. Talukdar, and H. Häffner, *Phys. Rev. B* **89**, 245435 (2014).
- [17] S. X. Wang, Y. Ge, J. Labaziewicz, E. Dauler, K. Berggren, and I. L. Chuang, *Appl. Phys. Lett.* **97**, 244102 (2010).
- [18] J. Chiaverini and J. M. Sage, *Phys. Rev. A* **89**, 012318 (2014).
- [19] J. B. Johnson, *Phys. Rev.* **32**, 97 (1928).
- [20] See Supplemental Material, which includes Refs. [27, 33–40].
- [21] M. Niedermayr, K. Lakhmanskiy, M. Kumph, S. Partel, J. Edlinger, M. Brownnutt, and R. Blatt, *New J. Phys.* **16**, 113068 (2014).
- [22] M. Niedermayr, *Cryogenic surface ion traps*, Ph.D. thesis, Leopold-Franzens-Universität Innsbruck (2015).
- [23] D. Leibfried, R. Blatt, C. Monroe, and D. Wineland, *Rev. Mod. Phys.* **75**, 281 (2003).
- [24] W. M. Itano, J. C. Bergquist, J. J. Bollinger, J. M. Gilligan, D. J. Heinzen, F. L. Moore, M. G. Raizen, and D. J. Wineland, *Phys. Rev. A* **47**, 3554 (1993).
- [25] J. B. Johnson, *Phys. Rev.* **32**, 97 (1928).
- [26] H. Nyquist, *Phys. Rev.* **32**, 110 (1928).
- [27] We use the electrode package for Python by R. Jördens (<https://github.com/nist-ionstorage/electrode>); see also [39, 40].
- [28] Datasets at temperatures  $T = (12, 41)$  K were each taken over the course of one day, the dataset at temperature  $T = 77$  K was taken over the course of 3 days.
- [29] W. A. Phillips, *Rep. Prog. Phys.* **50**, 1657 (1987).
- [30] V. Zhdanov, *Surf. Sci. Rep.* **12**, 185 (1991).
- [31] I. Talukdar, D. J. Gorman, N. Daniilidis, P. Schindler, S. Ebadi, H. Kaufmann, T. Zhang, and H. Häffner, *Phys. Rev. A* **93**, 043415 (2016).
- [32] D. Kielpinski, C. Monroe, and D. J. Wineland, *Nature* **417**, 709 (2002).
- [33] J. D. Jackson, *Classical electrodynamics*, 3rd ed. (Wiley, 1999).
- [34] H. Salamati and P. Kameli, *Physica B: Condensed Matter* **321**, 337 (2002).
- [35] R. A. Matula, *J. Phys. Chem. Rev. Data* **8**, 1147 (1979).
- [36] W. J. Carr, Jr, *AC loss and macroscopic theory of superconductors*, 2nd ed. (CRC Press, 2001).
- [37] D. Miller, P. L. Richards, S. Etemad, A. Inam, T. Venkatesan, B. Dutta, X. D. Wu, C. B. Eom, T. H. Geballe, N. Newman, and B. F. Cole, *Appl. Phys. Lett.* **59**, 2326 (1991).
- [38] G. Mikhailova, A. Prokhorov, A. Seferov, A. Troitskii, H. Freyhardt, J. Krelaus, N. Aleshina, N. Nizhelskii, and O. Polushchenko, *Solid State Commun.* **95**, 635 (1995).
- [39] R. Schmied, J. H. Wesenberg, and D. Leibfried, *Phys. Rev. Lett.* **102**, 233002 (2009).
- [40] R. Schmied, *New J. Phys.* **12**, 023038 (2010).

## SUPPLEMENTAL MATERIAL

### Skin depth in YBCO for $T > T_c$

The skin depth  $\zeta$  in a material is given by [33]

$$\zeta = \sqrt{\frac{2\rho}{\omega\mu}}, \quad (7)$$

where  $\rho$  is the resistivity of the material,  $\mu$  its permeability and  $\omega$  the frequency of the applied AC electric field. We calculate the resistivity  $\rho$  of our 50 nm-thick YBCO film from the 4-wire DC resistance measurement of the meander electrode (length 5.18 mm and width 10  $\mu\text{m}$ ). Taking a resistance  $R_m \approx 8 \text{ k}\Omega$  of the meander electrode above  $T_c$  (see Fig. 2 of the main text), we arrive at a resistivity  $\rho \approx 78 \times 10^{-8} \Omega\text{m}$ . Assuming  $\mu = \mu_0 = 2\pi \times 10^{-7} \text{ H m}^{-1}$  [34] and  $\omega = 2\pi \times 1.8 \text{ MHz}$  leads to a skin depth  $\zeta \approx 441 \mu\text{m}$ , which is much larger than the YBCO film thickness.

### Ruling out external technical noise

We rule out external technical noise as the origin of the ion heating rates for chip temperatures  $T < T_c$  (Fig. 4 of the main text). We note that the measured heating rates have a clear dependence on the trap chip temperature  $T$ . External technical noise sensed by the ion, on the other hand, does not depend on  $T$ , as we show in the following. The thermal decoupling incorporated in our setup ensures that while we locally heat the trap chip to temperatures  $T = (10 - 200) \text{ K}$ , the cryogenic environment, in particular the low-pass filters, stays at a nearly constant temperature  $T_f \approx (10 - 14) \text{ K}$ . The change in  $T_f$  is small, but it might still lead to a variation in the attenuation of external technical noise by the low-pass filters. Therefore, we measure the temperature dependence of the transfer function of the cryogenic low-pass filters. The filters, all identical, are placed only a few centimeters away from the trap and suppress noise that might reach the trap electrodes through the DC lines. The equivalent circuit of these first order RC filters is shown in Fig. 6(a). The filter consists of a resistor  $R_f = 100 \Omega$  (Vishay, Y1625100R000Q9R) and two capacitors  $C_a = 330 \text{ nF}$  (Kemet, C2220C334J1GACTU) and  $C_b = 470 \text{ pF}$  (Kemet, C0805C471J1GACTU) placed in parallel. Resistors  $R_a, R_b$  model the equivalent series resistance (ESR) of the capacitors. The capacitance of the trap electrode to ground  $C_{el}$  is on the order of 1 pF and negligible compared to the filter capacitance. The electrical setup for the measurement of the filter's transfer function is shown in Fig. 6(b). Two filters A and B are wire bonded to the same trap electrode. An RF signal with amplitude  $V_{in}$  is injected into filter A, and the attenuated signal  $V_{out}$  is measured at the input of filter

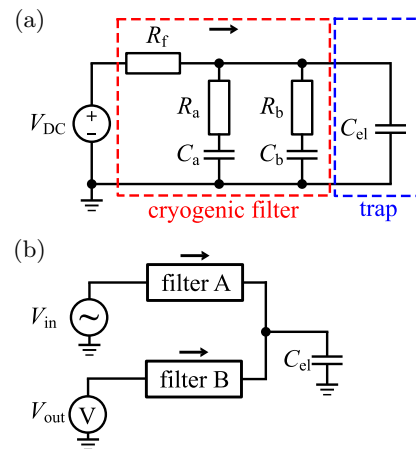


FIG. 6. (a) RC low-pass filter circuit used between the DC supplies and the trap electrodes. (b) Schematic layout of the circuit used for the measurement of the transfer function of the RC filters. The black arrows indicate the direction in which the filters act as low pass filters.

B. The transfer function measured in this configuration corresponds to that of the first order RC filter shown in Fig. 6(a), however with twice the filter capacitance  $C_{eff} \approx 2(C_a + C_b)$ . The additional capacitance reduces the cut-off frequency  $f_c \approx 4.8 \text{ kHz}$  by a factor of 2, which is irrelevant for the temperature scaling arguments used below. The resistance  $R_f$  of filter B can be neglected due to the high input impedance of 1 M $\Omega$  of the oscilloscope used to measure the output signal  $V_{out}$ . Additional filter effects arising from  $R_f$  of filter B and the outgoing cabling capacitance  $C_{cab} \approx 300 \text{ pF}$  are negligible due to a high cut-off frequency  $f_c \approx 5 \text{ MHz}$ , well above the frequency range of interest.

Fig. 7 shows the filter transfer function  $G = |V_{out}/V_{in}|^2$  for varying RC filter temperature  $T_f$  during cooling down and warming up of the entire cryogenic apparatus. The applied change in  $T_f$  strongly overestimates the variation in filter temperature  $T_f \approx (10 - 14) \text{ K}$  during the heating rate measurements. But even for stronger increase in  $T_f$ , the temperature scaling of the filter attenuation does not correlate with the heating rate data. Within the frequency range that is relevant for our experiment,  $\omega_z = 2\pi \times (0.4 - 1.8) \text{ MHz}$ , the low-pass filters show a slightly increasing attenuation for increasing temperature. This is likely due to an electric resonance caused by the parasitic inductance of the wiring and the low-pass filter capacitance. A noise source outside the cryostat penetrating through the low-pass filter lines would therefore produce a heating rate that decreases with rising temperature, in stark contrast to the behavior that we measure (Fig. 4 of the main text).

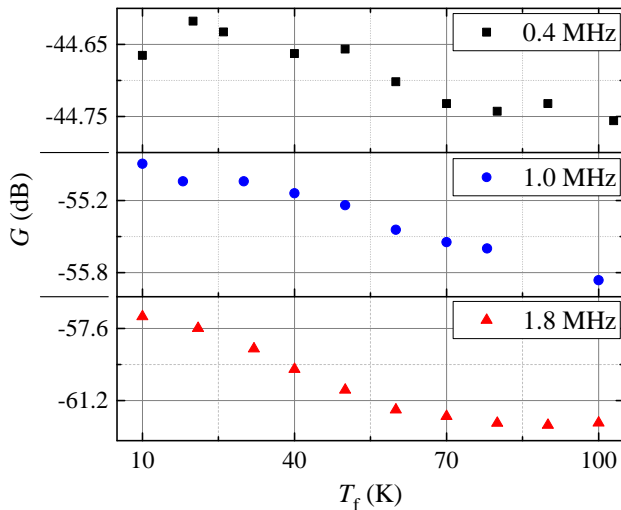


FIG. 7. Transfer function  $G$  of the cryogenic low-pass filters measured with the setup shown in Fig 6 (b) as a function of the filter temperature  $T_f$  at three different frequencies  $\omega = 2\pi \times (0.4, 1.0, 1.8)$  MHz.

### Ruling out Johnson noise for $T < T_c$

We exclude Johnson noise as dominant noise source for chip temperatures  $T < T_c$ . First, we exclude Johnson noise from the low-pass filters using a temperature scaling argument. As the trap chip is heated to  $T = 100$  K, the filter temperature changes by only  $\Delta T_f \approx 2$  K or roughly a factor 0.2, due to the thermal insulation. Assuming a constant filter resistance in the range  $\Delta T_f$ , Johnson noise scales linearly with temperature, see Eq. (2) of the main text. The electric field noise produced by the filters should therefore increase by about a factor 0.2 as well. In contrast, the increase of the measured noise level in Fig. 5 (b) of the main text from  $A = 2.0(1) \text{ V}^2/\text{m}^2$  at  $T = 12$  K to  $A = 7.7(3) \text{ V}^2/\text{m}^2$  at  $T = 77$  K corresponds to a change by roughly a factor 2.8, more than ten times larger than the change expected from Johnson noise from the filters. Second, we note that Johnson noise from the trap electrodes, bonding wires, and PCB traces, which are not filtered by the low-pass filters, should have a flat frequency dependence, see Eq. (2) of the main text. This is in clear contrast to the approximate  $1/f$  scaling found in our data, Fig. 4 of the main text.

In addition to the scaling arguments above, we explicitly calculate upper bounds for Johnson noise from trap electrodes, wiring, and low-pass filters. The contribution of Johnson noise produced by a resistance  $R(\omega, T)$  to the electric field noise  $S_E$  at the position of the ion is given by Eq. (2) of the main text. For all calculations we assume that the resistance of interest is connected to the trap electrode C1 (or equivalently C2) which has the smallest

characteristic distance  $\delta_c = 5.1$  mm of all trap electrodes [27].

Each trap electrode is connected to its first order RC filter via a gold wire bond and a gold-plated copper trace on the filter PCB. The wire bonds have a diameter of  $25 \mu\text{m}$  and a typical length of 1 cm. The wire bond resistance at  $T = 80$  K is then  $R_{\text{wb}} \approx 25 \text{ m}\Omega$ , using a typical resistivity  $\rho_{\text{Au}} \approx 0.48 \times 10^{-8} \Omega \text{ m}$  [35]. We neglect the contact resistance of the bonding wire to the chip and to the PCB trace. The traces have a width of  $300 \mu\text{m}$ , a thickness of  $100 \mu\text{m}$  and a maximal length of 2 cm to the first filter capacitor. The trace thickness is larger than the skin depth in copper  $\zeta_{\text{Cu}} \approx 26 \mu\text{m}$  at  $\omega = 2\pi \times 1.8 \text{ MHz}$ , calculated using Eq. (7) with a typical resistivity  $\rho_{\text{Cu}} \approx 0.22 \times 10^{-8} \Omega \text{ m}$  at  $T = 80$  K [35] and  $\mu = \mu_0$ . Therefore we use twice the skin depth instead of the trace thickness to calculate the trace resistance  $R_{\text{tr}} \approx 3 \text{ m}\Omega$  at  $T = 80$  K. The combined resistance of a trace and a wire bond at  $T = 80$  K is then  $R = R_{\text{wb}} + R_{\text{tr}} \approx 28 \text{ m}\Omega$ . The corresponding electric field noise  $S_E^{(\text{JN})} \approx 4.6 \times 10^{-18} \text{ V}^2 \text{ m}^{-2} \text{ Hz}^{-1}$  is two orders of magnitude smaller than the smallest noise level  $S_E = 5.2(11) \times 10^{-16} \text{ V}^2 \text{ m}^{-2} \text{ Hz}^{-1}$  we measure.

The resistances  $R_f, R_a, R_b$  within the RC filter circuit are another source of Johnson noise. The corresponding electric field noise is calculated by considering the effective real resistance  $R_{\text{eff}}$  of the circuit from the perspective of the trap electrode [6]. For the filter circuit shown in Fig. 6 (a) the effective real resistance is given by

$$R_{\text{eff}} = \Re \left\{ \left( \frac{-i}{\omega C_{\text{el}}} \right) \parallel \left( R_b - \frac{i}{\omega C_b} \right) \parallel \left( R_a - \frac{i}{\omega C_a} \right) \parallel R_f \right\}, \quad (8)$$

where  $a \parallel b$  denotes the impedance of two elements  $a, b$  in parallel. The ESR of the filter capacitors is frequency dependent. Within the relevant frequency range  $\omega_z = 2\pi \times (0.4 - 1.8) \text{ MHz}$  the maximal ESRs are  $R_a = 24(1) \text{ m}\Omega$  and  $R_b = 1.3(1) \Omega$  according to the room temperature specification of the capacitors. This gives rise to a maximal effective real resistance  $R_{\text{eff}} = 38(1) \text{ m}\Omega$ . The corresponding electric field noise at  $T = 80$  K,  $S_E^{(\text{JN})} = 6.5(2) \times 10^{-18} \text{ V}^2 \text{ m}^{-2} \text{ Hz}^{-1}$ , is two orders of magnitude smaller than the smallest noise level we measure.

We further give an upper bound for the amount of Johnson noise produced in the trap electrodes. In this calculation we neglect the influence of the electrodes' gold top layer, since the resistivity of gold is much higher than the resistivity of the YBCO film below it, which is small but finite in the RF domain, even below  $T_c$  [36]. The surface resistivity of the 50 nm thick YBCO film at  $f = 10.9 \text{ GHz}$  and  $T = 10$  K is  $\rho_{\text{YBCO}} \approx 0.66 \text{ m}\Omega$  (specified value  $\rho_{\text{YBCO}} \approx 0.1 \text{ m}\Omega$  for 330 nm thickness and  $T = 10$  K,  $f = 10.9 \text{ GHz}$ ; Ceraco ceramic coating GmbH, Ismaning, Germany). Extrapolating the known quadratic scaling of the resistivity with frequency [37]

down to the MHz regime, we calculate a surface resistivity  $\varrho_{\text{YBCO}} = 1.8 \times 10^{-11} \Omega$  at  $f = 1.8 \text{ MHz}$  and  $T = 10 \text{ K}$ . Further assuming a temperature scaling  $\varrho \propto (T/T_c)^2 / \sqrt{1 - (T/T_c)^4}$ , [38], we calculate a surface resistivity  $\varrho_{\text{YBCO}} = 3.4 \times 10^{-11} \Omega$  at  $f = 1.8 \text{ MHz}$  and  $T = 80 \text{ K}$ . In comparison, the 200 nm thick Au top layer even at  $T = 10 \text{ K}$  still has a surface resistivity of  $\varrho_{\text{Au}} = 1.1 \text{ m}\Omega$  [35]. From the YBCO surface resistivity we calculate the resistance of the trap electrodes for our trap geometry. We show here as an example the calculation for one of the meander-shaped electrodes. These electrodes have a length  $l = 5.18 \text{ mm}$  and a width  $w = 10 \mu\text{m}$ . The total meander resistance at  $f = 1.8 \text{ MHz}$  and  $T = 80 \text{ K}$  is then  $R_m = l\varrho_{\text{YBCO}}/w = 17.8 \text{ n}\Omega$ . The resistance of the other trap electrodes is calculated in an analog way. The total resistance of all trap electrodes in sum is  $R_{\text{tot}} = 56.5 \text{ n}\Omega$ . We assume that the total resistance  $R_{\text{tot}}$  is connected to the C1 electrode, which overestimates the influence of  $R_{\text{tot}}$  on the electric field noise at the ion position. The corresponding electric field noise at  $T = 80 \text{ K}$ ,  $S_E^{(\text{JN})} = 9.6 \times 10^{-24} \text{ V}^2 \text{ m}^{-2} \text{ Hz}^{-1}$ , is 7 or-

ders of magnitude smaller than the smallest noise level we measure.

#### **Influence of the YBCO meander electrodes on the ion heating rate for $T < T_c$**

We exclude any other potential effects of the superconducting YBCO meanders connected to C1 and C2 on the ion heating rate below  $T_c$ , like for instance electromagnetic pickup noise in the meander structure. For this we use a second, similar trap chip in which we compare the heating rate with electrodes C1 and C2 connected to the YBCO meanders (same configuration as for the experiment in the main text) or directly attached to the low-pass filters. We find no difference between these two configurations, and observe in both cases a heating rate  $\Gamma_h = 0.7(1) \text{ phonons/s}$  at  $\omega_z = 2\pi \times 1.0 \text{ MHz}$  and  $T = 14 \text{ K}$ , comparable to the value  $\Gamma_h = 0.23(2) \text{ phonons/s}$  at  $\omega_z = 2\pi \times 1.0 \text{ MHz}$  and  $T = 12 \text{ K}$  in Fig. 4 of the main text.